Mechanism of Formation of the Complex between Transferrin and Bismuth, and Interaction with Transferrin Receptor 1

Geneviève Miquel, Tarek Nekaa, Philippe H. Kahn, Miryana Hémadi, and Jean-Michel El Hage Chahine*

Interfaces, Traitements, Organisation et Dynamique des Systèmes, Université Paris 7-CNRS UMR 7086, 1 rue Guy de la Brosse, 75005 Paris, France

Received July 16, 2004; Revised Manuscript Received August 31, 2004

ABSTRACT: The kinetics and thermodynamics of Bi(III) exchange between bismuth mononitrilotriacetate (BiL) and human serum transferrin as well as those of the interaction between bismuth-loaded transferrin and transferrin receptor 1 (TFR) were investigated at pH 7.4−8.9. Bismuth is rapidly exchanged between BiL and the C-site of human serum apotransferrin in interaction with bicarbonate to yield an intermediate complex with an effective equilibrium constant K_1 of 6 ± 4, a direct second-order rate constant k_1 of (2.45 ± 0.20) × 10^5 M^{-1} s^{-1}, and a reverse second-order rate constant k_{-1} of (1.5 ± 0.5) × 10^6 M^{-1} s^{-1}. The intermediate complex loses a single proton with a proton dissociation constant K_{1a} of 2.4 ± 1 nM to yield a first kinetic product. This product then undergoes a modification in its conformation followed by two proton losses with a first-order rate constant $k_2 = 25 \pm 1.5$ s^{-1} to produce a second kinetic intermediate, which in turn undergoes a last modification in the conformation to yield the bismuth-saturated transferrin in its final state. This last process rate-controls Bi(III) uptake by the N-site of the protein and is independent of the experimental parameters with a constant reciprocal relaxation time τ_3^{-1} of (3 ± 1) × 10^{-2} s^{-1}. The mechanism of bismuth uptake differs from that of iron and probably does not involve the same transition in conformation from open to closed upon iron uptake. The interaction of bismuth-loaded transferrin with TFR occurs in a single very fast kinetic step with a dissociation constant K_d of 4 ± 0.4 μM, a second-order rate constant k_d of (2.2 ± 1.5) × 10^8 M^{-1} s^{-1}, and a first-order rate constant k_{-d} of 900 ± 400 s^{-1}. This mechanism is different from that observed with the ferric holotransferrin and implies that the interaction between TFR and bismuth-loaded transferrin probably takes place on the helical domain of the receptor which is specific for the C-site of transferrin and HFE. The relevance of bismuth incorporation by the transferrin receptor-mediated iron acquisition pathway is discussed.

Transferrins constitute the major iron transport system in vertebrates and invertebrates as they are also present in some bacterial species (*1*, *2*). Transferrins belong to the new protein transferrin superfamily that includes globular periplasmic transport proteins (*3*). Vertebrate soluble transferrins consist of a single amino acid chain of ∼700 units organized in two lobes, the C-lobe and the N-lobe. Each lobe contains an iron-binding cleft, in which the metal is coordinated to the two phenolates of two tyrosines, the carboxylate of an aspartate, and the imidazole of a histidine. The metal is also coordinated to a synergistic anion, which in natural media is a carbonate adjacent to an arginine (*4*, *5*). In neutral physiological media, when serum transferrin (ST)[1] is iron-loaded (holo-ST), it is recognized by transferrin receptor 1 (TFR) and to a lesser extent by transferrin receptor 2 (*1*, *2*, *6*, *7*). The protein adduct is internalized in the cytosol by receptor-mediated endocytosis, and iron is lost in an acidic endosome which is, then, recycled back to the cell surface where iron-free apotransferrin (apo-ST) is released into the biological fluid (*6*). We recently established the mechanism of interaction of ST with TFR. In neutral media, this interaction occurs in two steps. The first step is very fast and yields a kinetic product which undergoes, in the second step, a very slow change in conformation, allowing the holo-ST−TFR adduct to achieve its final equilibrated state with an overall dissociation constant of 2.3 nM (*7*).

* To whom correspondence should be addressed. Telephone: 33144276807. Fax: 33144276814. E-mail: chahine@paris7.jussieu.fr.

[1] Abbreviations: ST, serum transferrin; TFR, serum transferrin receptor 1; c_0, analytical transferrin receptor concentration; c_1, bismuth nitrilotriacetate concentration; c_2, analytical serum transferrin concentration; BiL, neutral bismuth mononitrilotriacetate; L^{3-} or NAc_3, nitrilotriacetate anion; $H_2T'_N-T'_CH_2$, apotransferrin, both sites of which are in an unknown state of protonation and charge; $H_2T'_N-T_CH_3$ and T_CH_3, apotransferrin in which only the C-site is interacting with bicarbonate; $H_3T_N-T_CH_3$, transferrin in which both sites are interacting with bicarbonate; T, transferrin in an unknown state; T_CH_3Bi, T_CH_2Bi, T_CBi, $H_jT_NT_CH_2Bi$, $TH_{j+2}TBi$, TH_jBi, and $T'H_jBi$, different C-site species of bismuth-loaded serum transferrin in an unknown state of charge, conformation, and protonation; TBi_2, $T'H_jBi$, and $T'H_jBi_2$, different species of bismuth-saturated serum transferrin in an unknown state of charge, conformation, and protonation; TFR, transferrin receptor 1 in an unknown state; $TFR-TBi_2$, transferrin receptor in an interaction with bismuth-loaded transferrin; TFe_2, holotransferrin in an unknown state; T_CH_3Fe, T_CHFe, $T_NH_3T_CH_2Fe$, TH_5Fe, $TH_{(5-m)}Fe$, $T'H_{(5-m)}Fe$, $T'H_{(4-m)}Fe$, and $T''H_{(4-m)}Fe$, different C-site species of iron-loaded serum transferrin in unknown states of charge, conformation, and protonation; $T'H_{(4-m)}Fe_2$ and $T''H_{(4-m)}Fe_2$, different species of iron-saturated serum transferrin in unknown states of charge, conformation, and protonation; $(TFR)-(TFe_2)$, kinetic intermediate of the receptor in an interaction with holotransferrin; $TFR-TFe_2$, receptor in an interaction with holotransferrin in the thermodynamically equilibrated state.

10.1021/bi048484p CCC: $27.50
Published on Web 10/30/2004

Transferrin is also known to form stable complexes with metals other than Fe(III) (*8*−*13*). This led to the involvement of transferrin in the transport of these metals, in their delivery to cells, and in the transport across the brain−blood barrier where their action was explained by their interference with the metabolism of iron (*2*). These metals can be toxic, such as aluminum, and/or useful in therapy or imagery such as bismuth or gallium (*8*−*13*). It can, nevertheless, be assumed that if the interaction of the metal-loaded transferrin with TFR does not occur, the metal transport to the cell will not follow this iron acquisition pathway.

We have established a general mechanism for the uptake of iron by the three major transferrins, human ST, bovine lactoferrin, and hen ovotransferrin (*15*−*17*). More recently, we established the mechanism of aluminum uptake by transferrin and showed that the aluminum-loaded ST does not interact with TFR (*9*).

Bismuth is widely used in medicine for the therapy of diarrhea and peptic ulcers (*18*). It is bactericidal, and its action against *Helicobacter pylori* is now recognized (*18*). *H. pylori* is responsible, among other things, for peptic ulcers and chronic active gastritis, and is suspected to be involved in gastric cancers (*10*−*12*, *18*). Furthermore, radioactive bismuth isotopes can also be used for targeted radiotherapy (*10*−*12*, *18*).

Bismuth strongly binds transferrins (*10*−*12*). The bismuth−transferrin complex may thus be internalized in the cytosol via the serum transferrin receptor iron acquisition pathway. However, the mechanism of formation of a complex between bismuth and ST is not yet well-known.

TFR is a homodimeric 190 kDa glycosylated membrane protein. Each of the two subunits possesses a transmembrane endodomain and an ectodomain of ∼700 amino acids directed toward the biological fluid. This ectodomain contains the transferrin-binding sites. It is composed of a helical domain, an apical domain, and a protease-like domain which is close to the transmembrane endodomain. The whole ectodomain can interact with two iron-loaded transferrins (*19*). A structure of the holo-ST−TFR ectodomain adduct with a precision of 7.5 Å was recently proposed and transposed to the whole protein, where it is suggested that the helical domain of TFR is the binding area of the C-lobe of holotransferrin, whereas the protease-like domain is that of the N-lobe (*20*). The amino residues involved in the binding of the protein were also proposed. They tended to confirm the existence of these two binding domains in each of the TFR subunits, one domain common to ST and the hemochromatosis protein (HFE), whereas the other is more specific for ST (*21*). What would then be the behavior of the bismuth-loaded transferrin toward the interaction with TFR? Would it occur by the same mechanisms as with holotransferrin, and would it match the proposed model?

In this article, by the use of the methods and techniques of chemical relaxation (*22*−*24*), we propose a mechanism for bismuth uptake by serum transferrin from the nitrilotriacetato−bismuth chelate ($BiNAc_3$) and analyze the interaction of the transferrin−bismuth complex with transferrin receptor 1.

EXPERIMENTAL PROCEDURES

More than 98% pure human serum apotransferrin (Sigma) was further purified by published procedures; its purity was checked spectrophotometrically, and by urea and SDS−polyacrylamide gel electrophoresis (*9*). KCl (Merck Suprapur), NaOH, HCl (Merck Titrisol), EDTA (Merck Titriplex), $FeCl_3$, trisodium citrate, acetic acid (96%), sodium acetate (Merck), sodium bicarbonate, glycerol, urea, SDS, boric acid, 3-[(3-cholamidopropyl)dimethylammonio]-1-propanesulfonate (CHAPS) (Ultra grade), dithiothreitol (DTT), phenylmethanesulfonyl fluoride (PMSF), Triton TX-100, ethanolamine, glycine (electrophoresis reagent), sodium azide (Sigma), lissamine rhodamine sulfonyl chloride (Acros), ammonium sulfate, nitrilotriacetic acid [$N(AcH)_3$], bromophenol blue, Brilliant blue, HEPES, bismuth subcarbonate [$(BiO)_2CO_3$] (Aldrich), acrylamide, APS, TEMED (Boehringer Mannheim), dibasic potassium phosphate trihydrate (Calbiochem), NaCl (molecular biology grade from Merck), and Sephadex G50 (Pharmacia) were used without further purification. Desferrioxamine was a gift from Novartis. Water and glassware were prepared as described previously (*24*).

Stock Solutions. The HEPES concentration in neutral buffers was 50 mM. Final pH values were continuously controlled and adjusted to between 7.2 and 8.6 with microquantities of concentrated HCl or NaOH. Transferrin concentrations (c_1) were spectrophotometrically checked and solutions diluted further to the required final concentrations in the buffers. Bismuth mononitrilotriacetate $BiNAc_3$ solutions were prepared according to published procedures while always avoiding the incubation of bismuth with >1 equiv of NAc_3 (*25*, *26*). All final ionic strengths were adjusted to 0.2 M with KCl.

Metal-Loaded Transferrins. The C-site iron-loaded and iron-saturated serum transferrin were prepared as described elsewhere (*8*, *9*, *15*−*17*, *27*). Bismuth-saturated transferrin was prepared by incubating ST overnight with ∼20-fold its concentration in $Bi(NAc_3)$ in the presence of 20 mM HCO_3^- at pH 7.4. The solution was afterward dialyzed 10 times against the final buffer. Protein purity was checked by SDS−PAGE, and the bismuth load was checked spectrophotometrically according to published procedures (*10*).

TFR Purification. TFR was extracted from human placenta and purified according to published procedures (*7*, *28*, *29*). Purity was checked by gradient SDS−PAGE (*7*). TFR was obtained pure and used complete without cleaving the endodomain. The TFR was labeled by six rhodamines outside the sites of interaction with transferrin, as described previously (*7*). Protein concentrations were determined spectrophotometrically and by a Bio-Rad protein assay. The final amount of TFR varied from 3 to 6 mg per placenta. TFR solutions were dialyzed four times against the final buffer. Final TFR concentrations (c_0) were achieved by dilution. Human placenta screened HIV-free and hepatitis C-free were provided by the maternity hospital of the town of Ivry.

Spectrophotometric Measurements. Absorption measurements were performed on a Cary 500 spectrophotometer equipped with a thermostated cell carrier. Fluorimetric measurements were performed on an Aminco-Bowman series 2 luminescence spectrometer equipped with a thermostated cell carrier. The spectra used for the static determination of equilibrium constants were recorded at the final equilibrated state (1−3 h after mixing).

Fast Kinetic Measurements. Kinetic runs occurring on the millisecond to second time scale were performed on a modified High-Tech SFL 5 stopped-flow apparatus equipped

with a thermostated bath held at 25 ± 0.5 °C, as described previously (*15*). Kinetic runs occurring in less than 1 ms were performed at a final temperature of 37 ± 1 °C on a modified Joule-effect Messanlagen und Studien absorption and fluorescence emission T-jump spectrophotometer, as described previously (*7*). All signals were accumulated at least 10 times and normalized.

Data Analysis. The data were analyzed as described previously (*7*, *9*). All the observed kinetics were pure mono- or multiexponential and assessed as relaxation modes (*22*−*24*). All experimental conditions were set to allow the use of the methods and techniques of chemical relaxation (*9*, *15*−*17*, *22*−*24*).

RESULTS

Apo-ST, holo-ST, bismuth-saturated ST, C-site bismuth-loaded ST, and TFR exhibit characteristic absorption and fluorescence emission spectra for an excitation wavelength (λ_{ex} = 280 nm) and an emission wavelength (λ_{em} > 300 nm) (*7*, *9*, *10*). Moreover, the TFR species labeled with six rhodamine moieties outside of its area of interaction with holo-ST possesses also other characteristic spectra for an excitation wavelength (λ_{ex} = 573 nm) and an emission maximum (λ_{em} = 593 nm) (*9*). To compare the results with those previously acquired with iron and aluminum (*7*, *9*, *15*), the experiments involving the uptake of bismuth by ST were performed at 25 ± 0.5 °C, whereas those involving the interaction of the bismuth-loaded ST with TFR were performed at 37 ± 1 °C. Furthermore, the charge of the protein species is not indicated, and the subscripts used for H are only relative values.

Kinetics of Uptake of Bismuth by Transferrin

When a solution of apotransferrin is rapidly mixed with >5 equiv of nitrilotriacetato−bismuth(III) ($BiNAc_3$ or BiL) in a stopped-flow apparatus, at least three kinetic processes are observed (Figure 1). The first is fast and occurs in the range of tens of milliseconds as an exponential decrease in the fluorescence emission with time (Figure 1A). It is followed by a second process which occurs in the range of hundredths of milliseconds as another exponential decrease in fluorescence emission with time (Figure 1B). As for the third process, it manifests as an exponential increase in the fluorescence emission which occurs in the range of 20 s (Figure 1B). At a fixed pH and HCO_3^- concentration, the first process depends on $BiNAc_3$ concentration (c_1) and on ST concentration (c_2), whereas the second process depends exclusively and indirectly on pH. These two processes are observed only when apotransferrin is mixed with $BiNAc_3$. They are not observed when a monoferric only C-site iron-loaded transferrin is mixed with $BiNAc_3$. The third process seems to be independent of the experimental parameters and occurs also with the C-site iron-loaded transferrin. The three kinetic processes of Figure 1 are not observed in the absence of HCO_3^-. Furthermore, we were not able to detect an exploitable signal for which $5c_2 \leq c_1$.

First Kinetic Process. Bicarbonate plays the role of a synergistic anion required for the uptake of bismuth (*10*−*12*). The interaction of ST with bicarbonate is extremely fast

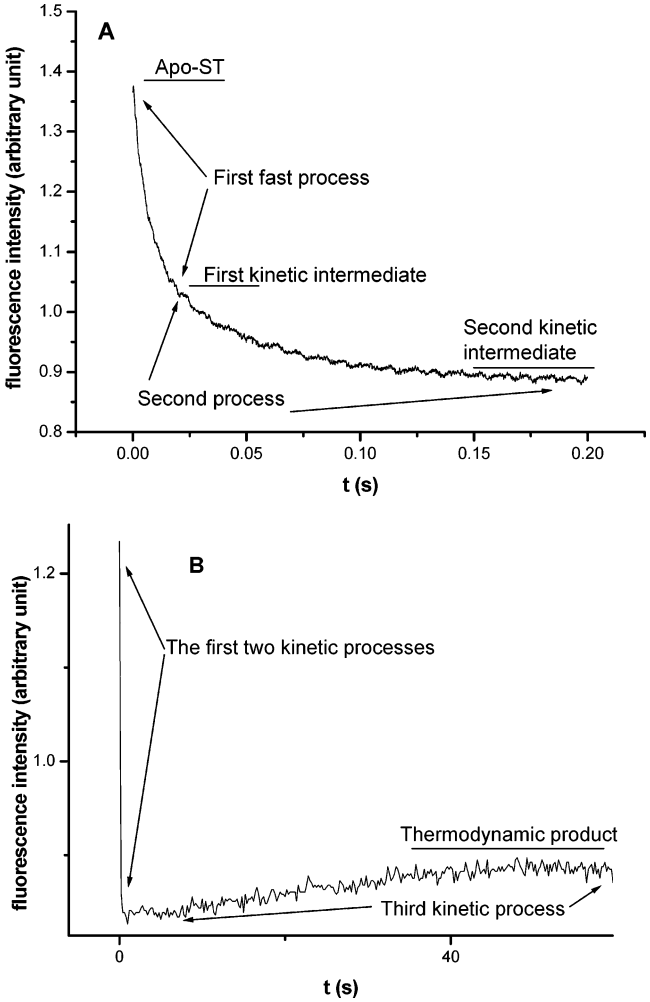

FIGURE 1: Variation of the fluorescence intensity with time after a fast stopped-flow mixing of a solution of ST (c_2 = 4 μM) with a solution of $BiNAc_3$ (c_1 = 0.4 mM) at pH 7.82 and 25 ± 0.1 °C where $[HCO_3^-]$ = 20 mM and μ = 0.2. Data in panel A were recorded between 0 and 0.5 s, and data in panel B were recorded between 0 and 50 s.

(eqs 1 and 2) and occurs with each of the C- and N-binding sites of ST (*30*).

$$H_2T'_N{-}T'_CH_2 + HCO_3^- \rightleftharpoons H_2T'_N{-}T_CH_3 \text{ (very fast)} \quad (1)$$

$$H_2T'_N{-}T_CH_3 + HCO_3^- \rightleftharpoons T \text{ (very fast)} \quad (2)$$

where $H_2T'_N{-}T'_CH_2$ is the protein not interacting with bicarbonate, $H_2T'_N{-}T_CH_3$ is the protein of which only the C-site is interacting with bicarbonate (hereafter represented as T_CH_3), and T is the protein in an unknown state.

The dissociation constant of the bicarbonate−C-site ST adduct ($K_{Cbic} = [H_2T'_N{-}T'_CH_2][HCO_3^-]/[T_CH_3]$ = 4.35 mM) is approximately one-tenth of that of the bicarbonate−N-site adduct ($K_{Nbic} = [H_2T'_N{-}T_CH_3][HCO_3^-]/[T]$ = 36 mM). Therefore, in neutral physiological media ($[HCO_3^-] \sim$ 20 mM), the interaction with bicarbonate occurs mainly with the C-site of the protein (*30*). This added to the fact that the interaction with bicarbonate is a prerequisite for metal uptake can explain why, in the case of iron and aluminum, the initial metal uptake by ST always occurs with the C-site interacting with bicarbonate (*9*, *15*−*17*). On the other hand, the fact that the affinity of the C-site for bismuth is higher than that

of the N-site (*12*) led us to assume that formation of a complex between Bi(III) and ST primarily takes place on the C-site of the protein. Three possible paths can describe this first metal uptake by ST (*9*, *15*−*17*). At a fixed pH and HCO_3^- concentration, we shall start by roughly considering two of the three possibilities which can describe this initial metal uptake (*9*, *15*−*17*).

In the first, the fastest step in Figure 1A is ascribed to the formation of a ternary complex between ST and $BiNAc_3$ (*9*, *17*, *24*).

$$T + BiL \rightleftharpoons TBiL \quad (3)$$

In the second case, metal exchange between the chelate and the protein occurs after chelate dissociation (eqs 4 and 5) (*24*).

$$Bi^{3+} + L^{3-} \rightleftharpoons BiL \quad (4)$$

$$Bi^{3+} + T \rightleftharpoons TBi \quad (5)$$

Equations 3−5 were investigated as previously described for Fe(III) and Al(III) (*9*, *15*−*17*). They were found to be inadequate and were discarded.

We, therefore, assumed that the first step in bismuth uptake occurs by a reaction similar to that reported for iron exchange between an iron chelate and the protein (*9*, *15*−*17*). At a fixed pH and HCO_3^- concentration, this can be approximately expressed by eq 6.

$$T + BiL \underset{k'_{-obs}}{\overset{k'_{obs}}{\rightleftharpoons}} TBi + L^{3-} \quad (6)$$

At a fixed pH of 5 and a constant c_2 where $c_1 > c_2$ and no added nitrilotriacetate anion, the reciprocal relaxation time equation associated with eq 6 can be expressed as eq 7 (*9*, *15*−*17*).

$$\tau_1^{-1} \approx k'_{obs}(c_1 - c_2) + k''_{-obs}2c_2 \quad (7)$$

Equation 7 is respected, as shown by the linear least-squares regression of τ_1^{-1} against $c_1 - c_2$ (Figure 2). This implies that the first step in bismuth uptake by ST is a metal exchange between the chelate and the protein.

The dependence of the experimental reciprocal relaxation times, related to the first step of Figure 1A, on pH and HCO_3^- concentration leads us to assume that the exchange of Bi(III) between the bismuth chelate ad ST involves, as in the case of iron, one or several proton dissociations. This can be expressed by eqs 8 and 9 (*15*−*17*).

$$T_CH_3 + BiL \underset{k_{-1}}{\overset{k_1}{\rightleftharpoons}} T_CH_3Bi + L^{3-} \text{ (rate-limiting)} \quad (8)$$

$$T_CH_3Bi \rightleftharpoons T_CH_{3-m}Bi + mH^+ \text{ (fast)} \quad (9)$$

where m is the number of protons lost in eq 9, $K_1 = [T_CH_3Bi][L]/[T_CH_3][BiL]$, and $K_{1a} = [H^+]^m[T_CH_{3-m}Bi]/[T_CH_3Bi]$. Under our experimental conditions where $c_1 \geq 10c_2$, $[BiL] \approx c_1 - c_2$, and $[L^{3-}] \approx c_2$ and since $[T_CH_3Bi] = c_1/(1 + K_{1a}/[H^+]^m)$, the reciprocal relaxation time associated with rate-limiting eq 8 is expressed as eq 10 (*15*−*17*).

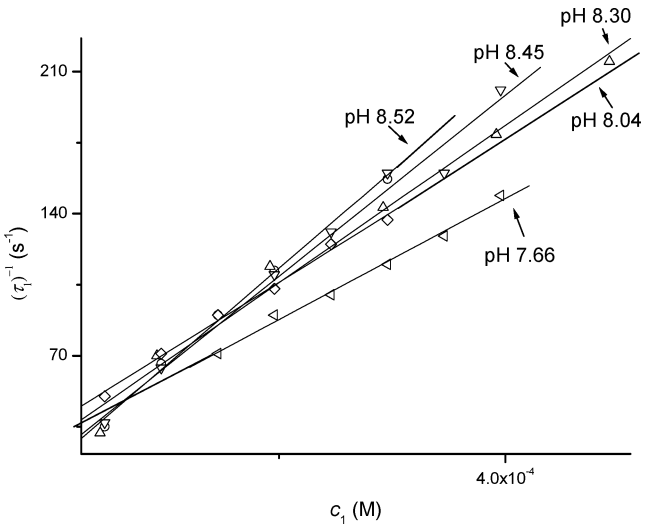

FIGURE 2: Plot of τ_1^{-1} against c_1 at 25 ± 0.5 °C, $\mu = 0.2$, and five fixed pH values. pH 7.66: intercept of 28 ± 7 s^{-1}, slope of (3.0 ± 0.3) × 10^5 M^{-1} s^{-1}, $r = 0.99625$, and $c_2 = 4$ μM. pH 8.04: intercept of 35 ± 5 s^{-1}, slope of (3.5 ± 0.3) × 10^5 M^{-1} s^{-1}, $r = 0.99698$, and $c_2 = 4$ μM. pH 8.30: intercept of 30 ± 14 s^{-1}, slope of (3.9 ± 0.4) × 10^5 M^{-1} s^{-1}, $r = 0.99259$, and $c_2 = 8$ μM. pH 8.45: intercept of 20 ± 14 s^{-1}, slope of (4.4 ± 0.4) × 10^5 M^{-1} s^{-1}, $r = 0.99219$, and $c_2 = 4$ μM. pH 8.52: intercept of 17 ± 7 s^{-1}, slope of (4.8 ± 0.2) × 10^5 M^{-1} s^{-1}, $r = 0.99773$, and $c_2 = 4$ μM.

$$\tau_1^{-1}/2c_2 = k_{-1} + k_1(c_1 - c_2)(1 + K_{1a}/[H^+]^m)/(\gamma^2 c_2) \quad (10)$$

where $\gamma = 1 + K_{bic}/[HCO_3^-]$.

At a fixed pH and HCO_3^- concentration, in the absence of nitrilotriacetate, and at a constant c_2, eq 10 can also be expressed as eq 11.

$$\tau_1^{-1} = k_{-1}2c_2 + k_{obs}(c_1 - c_2)/\gamma \quad (11)$$

for which

$$k_{obs} = k_1K_{1a}/[H^+]^m + k_1 \quad (12)$$

At a fixed pH of 5, a fixed c_2, and a fixed HCO_3^- concentration, five k_{obs} values were determined from the slope of the five regression lines of Figure 2 and γ. A good linear regression of k_{obs} against eq 12 is only obtained when $m = 1$ (Figure 3). From the slope and intercept of the best line, we determined $k_1 = (2.75 \pm 0.20) \times 10^5$ M^{-1} s^{-1} and $K_{1a} = 2.40 \pm 0.10$ nM. This last value is lower than that reported for the same proton loss occurring during iron uptake from two different iron chelates (nitrilotriacetate and acetatohydroxamate) (*9*, *15*). k_1 is higher than that reported for iron, which implies that bismuth uptake by transferrin is a little faster than that of iron. A linear least-squares regression of experimental data acquired between pH 7.44 and 8.52, at a c_1 between 50 μM and 0.5 mM, at a c_2 of 4 or 8 μM, and at a HCO_3^- concentration of 20 or 40 mM against eq 10 was obtained (Figure 4). From the slope and intercept of the best

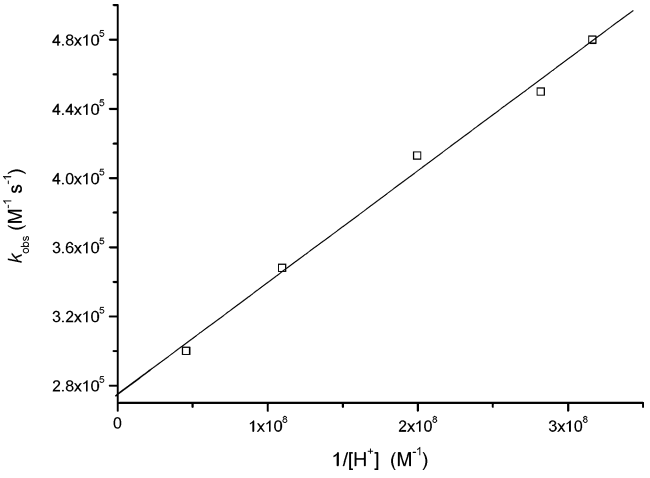

FIGURE 3: Plot of k_{obs} against $1/[H^+]$. Intercept = $(3.3 \pm 1.0) \times 10^9$ M^{-1} s^{-1}. Slope = 35 ± 5 s^{-1}. $r = 0.992204$.

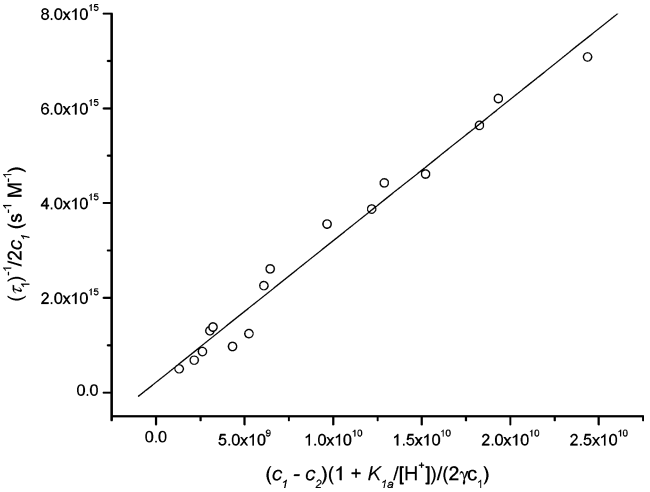

FIGURE 4: Plot of $\tau_1^{-1}/2c_1$ against $(c_1 - c_2)(1 + K_{1a}/[H^+])/(2c_1\gamma)$ for $c_2 = 4$ or 8 μM, $[HCO_3^-] = 20$ or 40 mM, $7.44 \leq$ pH ≤ 8.52, 50 $\mu M \leq c_1 \leq 0.5$ mM, and $\mu = 0.2$ at 25 ± 0.5 °C. Intercept = $(1.5 \pm 1.0) \times 10^6$ M^{-1} s^{-1}. Slope = $(2.45 \pm 0.20) \times 10^5$ M^{-1} s^{-1}. $r = 0.98838$.

regression line,the following values were determined: $k_1 = (2.45 \pm 0.20) \times 10^5$ M^{-1} s^{-1}, $k_{-1} \approx (1.5 \pm 0.5) \times 10^6$ M^{-1} s^{-1}, and $K_1 = k_{-1}/k_1 = 6 \pm 4$. Our experiments were performed with the bismuth−mononitrilotriacetate complex in the absence of the dinitrilotriacetate complex (*25*, *26*). This implies that at the end of this fast process, the affinity of ST for Bi(III) (eq 8) is on the same order of magnitude as that of one nitrilotriacetate for the same metal. Assuming that for the bismuth mononitrilotriacetate $BiNAc_3$ complex, $\log \beta_{BiL} = \log([BiNAc_3]/[Bi^{3+}][NAc_3^{3-}]) = 18.2$ (*31*), this would give $[Bi^{2+}][T_CH_3]/[T_CH_3Bi] = K_1K_L \approx (4 \pm 3) \times 10^{-18}$ M, which gives for the transferrin bismuth complex at the end on the first kinetic step the following: $\log \beta = -\log(K_1K_L) = 17.4 \pm 1.0$.

Second Kinetic Process. In the second kinetic process of Figure 1, the first kinetic intermediate T_CH_2Bi yields a second intermediate (Figure 1). The experimental reciprocal relaxation times associated with this second process of Figure 1B (τ_2^{-1}) depend on only pH, as observed for the first change in conformation following the uptake of iron or aluminum by ST (*15*−*17*). We, therefore, ascribed this second process to rate-limiting eq 13, in which T_CH_2Bi undergoes a

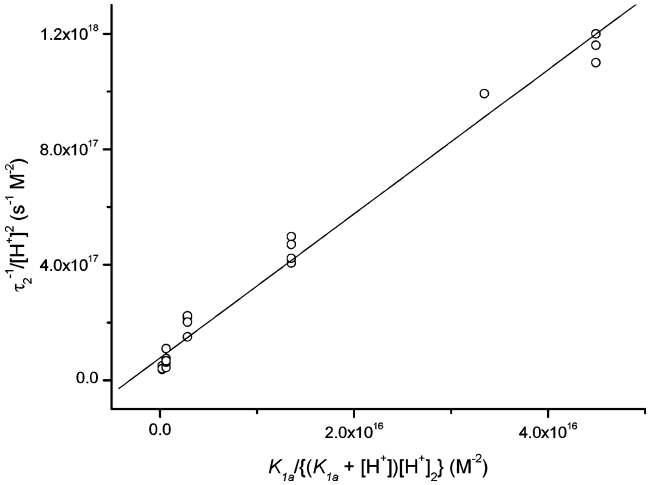

FIGURE 5: Plot of $t_2^{-1}/[H^+]^2$ against $K_{1a}/[(K_{1a} + [H^+])[H^+]^2]$ for $c_2 = 4$ or 8 μM, $[HCO_3^-] = 20$ or 40 mM, $7.44 \leq$ pH ≤ 8.52, 50 $\mu M \leq c_1 \leq 0.5$ mM, and $\mu = 0.2$ at 25 ± 0.5 °C. Intercept = $(7.7 \pm 2.0) \times 10^{16}$ M^{-2} s^{-1}. Slope = 25.0 ± 0.5 s^{-1}. $r = 0.99085$.

modification in conformation followed by l diffusion-controlled proton losses (*15*−*17*).

$$T_CH_2Bi \underset{k_{-2}}{\overset{k_2}{\rightleftharpoons}} T'_CH_2Bi \quad (13)$$

$$T'_CH_{2-l}Bi + lH^+ \rightleftharpoons T'_CH_2Bi \quad (14)$$

where T'_CH_2Bi is the second intermediate for which $K_{2a} = [T'_CH_{2-l}Bi][H^+]^l/[T'_CH_2Bi]$ and $K_2 = [T'_CH_2Bi]/[T_CH_2Bi]$.

The reciprocal relaxation time equation associated with rate-limiting eq 13 can be expressed as (*15*)

$$\tau_2^{-1}/[H^+]^l = k_2K_{1a}/[(K_{1a} + [H^+])[H^+]^l] + k_{-2}/K_{2a} \quad (15)$$

A good linear regression of the data against eq 15 was only obtained for $l = 2$ (Figure 5). A k_2 of 25 ± 1.5 s^{-1} and a k_{-2}/K_{2a} of $(7.7 \pm 2) \times 10^{16}$ M^{-2} s^{-1} were determined from the slope and intercept of the best regression line. The k_2 value is practically 1 order of magnitude higher than that for the uptake of iron. The second modification in conformation of the protein is, therefore, accompanied by the loss of two protons. The overall proton dissociation constant associated with eqs 13 and 14 can be expressed as $K'_{2a} = K_{2a}k_2/k_{-2} = [T_CH_{2-l}Bi][H^+]^2/[T'_CH_2Bi] = 3.25 \times 10^{-16}$ M^2.

Third Kinetic Process. In the third kinetic process of Figure 1B, the second kinetic intermediate $T'_CH_{2-l}Bi$ yields the final spectrophotometrically identified thermodynamically stable bismuth-saturated ST species (TBi_2) (*10*). This final process occurs with a reciprocal experimental relaxation time τ_3^{-1} of $(3 \pm 1) \times 10^{-2}$ s^{-1}. It does not seem to depend on any of the experimental parameters (pH, c_1, and c_2). It occurs in ~50 s and seems to rate-control the uptake of a second bismuth by the ST. Furthermore, the fact that the measured τ_3^{-1} values are independent of the concentrations of the species present in the medium indicates that within the experimental uncertainties, this final kinetic process is associated with a monomolecular reaction, such as a change in conformation (*15*−*17*, *22*, *23*). Therefore, we shall associate the slow kinetic process of Figure 1B with a final change in the conformation of ST, during which the metal-loaded protein attains its final state of equilibrium.

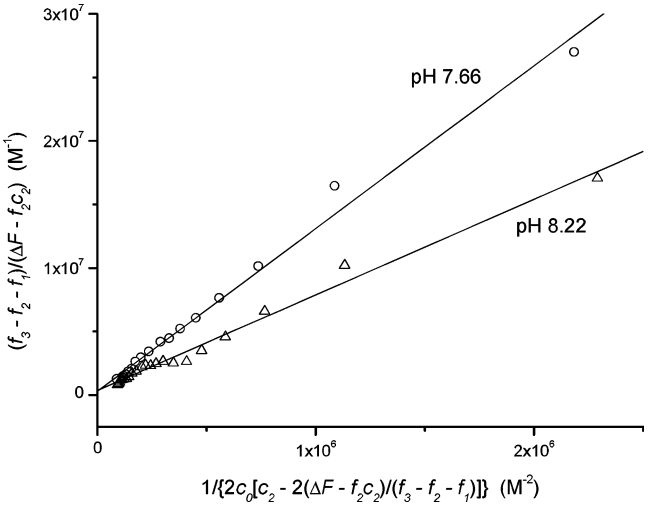

FIGURE 6: Plot of $(f_3 - f_2 - f_1)/(\Delta F - f_2c_2)$ against $1/\{2c_0[c_2 - 2(\Delta F - f_2c_2)/(f_3 - f_2 - f_1)]\}$ at two fixed pH values, where $c_0 = 0.45\ \mu$M, $0.5\ \mu\text{M} \leq c_2 \leq 15\ \mu$M, and $\mu = 0.2$ at 37 ± 1 °C. pH 7.66: intercept of $(3 \pm 4) \times 10^5\ \text{M}^{-1}$, slope of 12.8 ± 0.7, and $r = 0.99499$. pH 8.22: intercept of $(3.5 \pm 2.5) \times 10^5\ \text{M}^{-1}$, slope of 7.4 ± 0.4, and $r = 0.99373$.

Interaction of Bismuth-Loaded Transferrin with TFR

TFR consists of two identical subunits, each of which contains interaction sites with one ST (*19*, *20*). Therefore, our analysis deals with interaction site concentration ($2c_0$) and not with the TFR concentration (c_0).

At a fixed pH value, adding TBi_2 to TFR in the presence of 1% CHAPS leads to a decrease in fluorescence intensity accompanied by a red shift in the emission maximum. Similar spectral modifications were also observed with iron-loaded transferrin in, however, a concentration range ~3 orders of magnitude lower than that used here for the bismuth-loaded ST. As with iron-loaded ST, we associate this fluorescence variation with the molecular interaction of the receptor with bismuth-loaded ST (eq 16).

$$(\text{TFR}) + \text{TBi}_2 \rightleftharpoons (\text{TFR})-(\text{TBi}_2) \qquad (16)$$

where TBi_2 is the bismuth-saturated ST in neutral media in an unknown state of protonation and charge, (TFR) is the transferrin receptor, (TFR)−(TBi_2) is a TBi_2−TFR adduct in unknown states, and $K_{obs} = [(\text{TFR})][\text{TBi}_2]/[(\text{TFR})-(\text{TBi}_2)]$.

At a fixed pH value, the variation in fluorescence emission intensity of a solution of TFR and TBi_2 at the final equilibrated state obeys eq 17 (*9*).

$$(f_3 - f_2 - f_1)/(\Delta F - f_2c_2) = {}^1/_2c_0 + K_{obs}/\{2c_0[c_2 - 2(\Delta F - f_2c_2)/(f_3 - f_2 - f_1)]\} \qquad (17)$$

in which f_1−f_3 are the experimental proportionality factors that link the fluorescence emission to [(TFR)], [TBi_2], and [(TFR)−(TBi_2)], c_0 is the TFR concentration, F_0 is the fluorescence intensity of TFR in the absence of transferrin, and F is the fluorescence intensity ($\Delta F = F - F_0$).

Figure 6 shows a linear least-squares regression of the data against eq 17 for the bismuth-saturated ST in the presence of 1% CHAPS at two fixed pH values (7.60 and 8.22). From the slope of the best regression lines and c_0, two apparent dissociation constants (K_{obs}) are determined ($11.5 \pm 1.0\ \mu$M at pH 7.60 and $6.8 \pm 0.6\ \mu$M at pH 8.22). These K_{obs} values are 3−4 orders of magnitude higher than those reported for the interaction of $STFe_2$ with TFR under similar conditions (*7*).

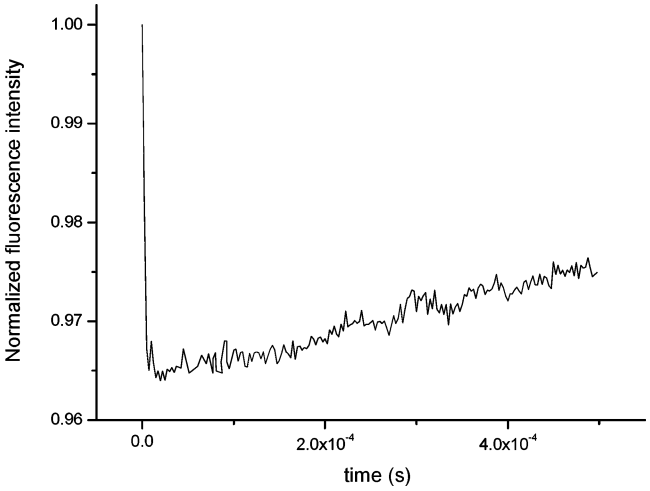

FIGURE 7: Fluorescence intensity variation with time after a temperature jump from 25 to 37 ± 1 °C performed on a TFR solution ($c_0 = 0.45\ \mu$M) at pH 7.44 in the presence of TBi_2 ($c_2 = 3.6\ \mu$M for $\lambda_{ex} = 280$ nm and $\lambda_{em} > 300$ nm and $\mu = 0.2$).

In the vicinity of neutrality, TFR exists in two prototropic states, TFR and TFRH. We have shown that only the basic species TFR interacts with holotransferrin (*7*). This led us to assume that this is also the case with TBi_2 (eqs 18 and 19).

$$\text{TFR} + \text{H}^+ \rightleftharpoons \text{TFRH} \qquad (18)$$

$$\text{TFR} + \text{TBi}_2 \underset{k_{-d}}{\overset{k_d}{\rightleftharpoons}} \text{TFR}-\text{TBi}_2 \qquad (19)$$

where $K_d = [\text{TFR}][\text{TBi}_2]/[\text{TFR}-\text{TBi}_2]$ and $K_a = [\text{TFR}][\text{H}^+]/[\text{TFRH}] = 10$ nM (*7*).

In this case, K_{obs} can be expressed via eq 20 (*7*).

$$K_{obs} = K_d + K_d[\text{H}^+]/K_a \qquad (20)$$

Knowing K_{obs} and K_a, we can easily determine K_d. Both K_{obs} values measured at pH 7.60 and 8.22 gave within the limits of uncertainty the same K_d ($4.0 \pm 0.4\ \mu$M). This value is more than 3 orders of magnitude higher than that reported for the TFR−holo-ST protein adduct (2.3 nM) (*7*).

Kinetics of the Interaction of Bismuth-Loaded ST with TFR. When a solution of TFR and TBi_2 is subjected to a fast temperature jump, two kinetic processes are detected. The first process is not resolved by the temperature-jump technique. It occurs as an extremely fast decrease in the fluorescence emission (≤200 ns), whereas the second occurs in the 500 μs range as an exponential increase in the fluorescence emission (Figure 7). These two processes are observed with both native and rhodamine-labeled TFR. Under similar conditions, with both the native and labeled proteins, the experimental reciprocal relaxation times $(\tau_4)^{-1}$ associated with the second process of Figure 7 are, within the limits of uncertainty, identical. This implies that the rhodamine labeling does not affect the kinetic analysis. We did not detect any other slow process as during the interaction between holo-ST and TFR (*7*).

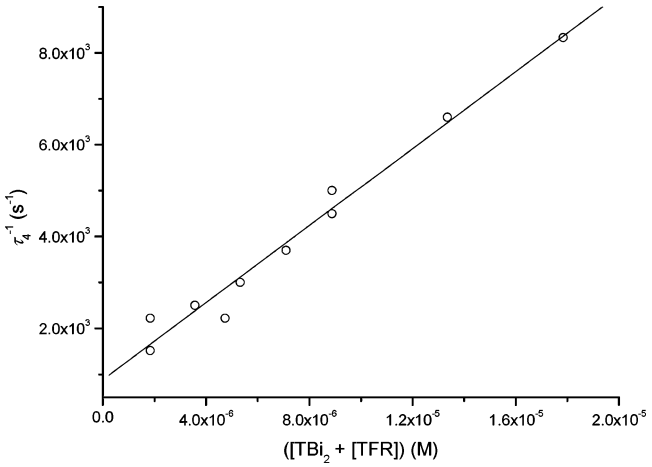

FIGURE 8: Plot of τ_4^{-1} against [TBi_2] + [TFR]. Intercept = 900 ± 400 s^{-1}. Slope = (2.5 ± 1.5) × 10^8.

Moreover, when a temperature jump is performed on a solution containing TBi_2 in excess and TFR just after the addition of holotransferrin, we only observe the two fast kinetic phenomena (200 ns and 50 μs) related to the interactions of TFR with the CHAPS micelles and with holo-ST (*7*). On the other hand, a temperature jump, performed on a solution containing TFR and holo-ST in the final equilibrated state after the addition of TBi_2, shows, as in the absence of TBi_2, only the ultrafast kinetic process (200 ns) related to the interaction between the final thermodynamic holo-ST−TFR species with CHAPS micelles (*7*). In both cases, everything happens as in the absence of TBi_2.

Proton transfer reactions are usually diffusion-controlled with second-order rate constants in the range of 10^{10} M^{-1} s^{-1} (*7*, *22*, *23*). Therefore, under our experimental conditions in buffered media between pH 8.10 and 7.44, the relaxation times associated with these reactions would be in the millisecond range (*7*). In the case of the second step of Figure 7, the relaxation times (τ_4) associated with the second kinetic process of Figure 7 are in the range of 100 μs, and the reciprocal relaxation times (τ_4^{-1}) depend on c_0 and c_1 and do not depend directly on [H^+]. They cannot, therefore, be ascribed to a proton transfer (*22*, *23*). They can, however, be associated with the molecular interaction between TBi_2 and the binding site of each of the TFR subunits (eq 19). This leads to eq 21 (*22*, *23*).

$$\tau_4^{-1} \approx k_{-d} + k_d(c_2 - 2c_0 + [TFR]) \qquad (21)$$

with [TFR] as the positive solution of quadratic eq 22 (*7*).

$$(2c_0 - c_2)(1 + [H^+]/K_a)K_d + [2c_0 - c_2 + (1 + [H^+]/K_a)K_d][TFR] + [TFR]^2 = 0 \quad (22)$$

We obtained good linear least-squares regression of the experimental reciprocal relaxation times associated with the second kinetic process of Figure 7 (Figure 8). From the slope and intercept, the following values were determined: k_d = (2.2 ± 1.5) × 10^8 M^{-1} s^{-1}, k_{-d} = 900 ± 400 s^{-1}, and K_d = 4 ± 2 μM. The K_d value is within the limits of uncertainty, equal to that determined spectrophotometrically at thermodynamic equilibrium after mixing TFR with TBi_2. This implies that the interaction between TFR and TBi_2 occurs in a single fast step.

DISCUSSION

The bismuth exchange experiments were performed with ST and bismuth−mononitrilotriacetate $BiNAc_3$ while always avoiding the presence of the bismuth−dinitrilotriacetate species [$Bi(NAc_3)_2$] (*25*, *26*). The speciation of $BiNAc_3$ is simple with the presence of a single $BiNAc_3$ species in neutral media (*25*, *26*). Moreover, the dissociations of $BiNAc_3$ and $FeNAc_3$ are fast (*15*, *25*). Therefore, the kinetics of iron or bismuth exchange are controlled by metal exchange between the chelate and apo-ST (eq 8, Table 1) and not by chelate dissociation.

In Table 1, we summarize the mechanism of bismuth exchange between $BiNAc_3$ and apotransferrin in neutral media. With iron, we were able to investigate metal uptake by only the C-site of the protein when the iron ligand concentration was equal to or lower than that of transferrin. We, moreover, showed a cooperativity between the sites upon iron uptake (*15*−*17*). With bismuth, we were not able to investigate uptake of a single metal by transferrin, as we were only able to analyze the data acquired when $5c_2 \leq c_1$. Therefore, despite the fact that the final affinity of ST for bismuth is lower than that for iron (*10*), we had to presume, as for iron uptake by ovotransferrin (*17*), that during the first steps in the exchange of bismuth between $BiNAc_3$ and apotransferrin (Figure 1A), the equilibrium is shifted toward $BiNAc_3$. This is confirmed by the lower log β (17.4) value for the ST−Bi intermediate complex as compared to the log β_{BiL} of $BiNAc_3$ (18.2) (eq 26, Table 1). The affinity of the C-site of ST for Bi(III) is higher than that of the N-site, and the C-site bismuth-loaded ST has been isolated (*10*). Furthermore, the first two kinetic processes of Figure 1 are not observed during bismuth uptake by the N-site of a monoferric C-site-only iron-loaded transferrin. This led us to ascribe these two kinetic processes to bismuth uptake by the C-site of ST (eqs 8, 9, 13, and 14, Table 1). The first step in the acquisition of bismuth by ST is very fast and occurs in the range of tens of milliseconds (Figure 1A). We ascribed it to metal exchange between $BiNAc_3$ and the C-site of apotransferrin in interaction with bicarbonate. Formation of this first bismuth complex is followed by a proton loss with a pK_{1a} of 8.6 to yield kinetic intermediate T_CH_2Bi (eq 9, Table 1). T_CH_2Bi undergoes, then, a change in conformation followed by the loss of two protons (eqs 13 and 14, Table 1). The third kinetic process of Figure 1B is independent of all the concentrations of the species present in the medium. It is ascribed to a monomolecular change in conformation of the bismuth-loaded protein during which it attains its final state of equilibrium. However, this process is observed when $BiNAc_3$ reacts with a C-site-only iron-loaded or an N-site iron-free transferrin. This implies that this final process rate-controls the uptake of bismuth by the N-site (eqs 23−26, Table 1). This final change in conformation, which occurs in the range of 50 s, is much faster than the final change in conformation, which occurs upon iron uptake and which takes ~1 h (Table 1). Thus, under similar conditions, uptake of bismuth by ST is more than 60 times faster than that of iron.

Fe(III) is considered a hard metal which forms stable complexes with oxygen-containing ligands (*32*), whereas Bi(III) is considered a borderline metal which forms stable

Table 1: Mechanisms of Bismuth and Iron Exchange between the Nitrilotriacetate Complexes and Human Serum Apotransferrin[a]

reaction	average direct rate constant	average reverse rate constant	equilibrium constant
$T'_CH_2 + HCO_3^- \rightleftharpoons T_CH_3$ (1)			4.35 mM
bismuth uptake			
$T_CH_3 + BiL \rightleftharpoons T_CH_3Bi + L$ (8)	$(2.45 \pm 0.20) \times 10^5\ M^{-1}\ s^{-1}$	$(1.5 \pm 0.5) \times 10^6\ M^{-1}\ s^{-1}$	6 ± 4
$T_CH_3Bi \rightleftharpoons TCH_2Bi + H^+$ (9)			2.4 ± 0.10 nM
$H_jT_NT_CH_2Bi \rightleftharpoons TH_{j+2}Bi$ (13)	$25 \pm 1.5\ s^{-1}$		
$TH_jBi + 2H^+ \rightleftharpoons TH_jBi$ (14)			
$TH_jBi \rightleftharpoons T'H_jBi$ (23)			
$T'H_jBi + BiL \rightleftharpoons L + T'H_jBi_2$ (24)			
$T'H_jBi_2 \rightleftharpoons T''H_jBi_2$ (25)			
$T_CH_3 + Bi^{3+} \rightleftharpoons T_CH_3Bi$ (26)			$(1.5 \pm 1) \times 10^{-17}$ M
iron uptake			
$T_CH_3 + FeL' \rightleftharpoons T_CH_3Fe + L$ (27)	$8.0 \times 10^4\ M^{-1}\ s^{-1}$	$7.5 \times 10^4\ M^{-1}\ s^{-1}$	1.00
$T_CH_3Fe \rightleftharpoons T_CH_2Fe + H^+$ (28)			16 nM
$H_3T_NT_CH_2Fe \rightleftharpoons TH_5Fe$ (29)	$2.80\ s^{-1}$		
$TH_5Fe \rightleftharpoons TH_{(5-l)}Fe + lH^+$ (30)			
$T'H_{(5-m)}Fe \rightleftharpoons TH_{(5-l)}Fe$ (31)	$6.2 \times 10^{-2}\ s^{-1}$		
$T'H_{(4-m)}Fe + H^+ \rightleftharpoons T'H_{(5-l)}Fe$ (32)			6.8 nM
$T'H_{(4-m)}Fe \rightleftharpoons T''H_{(4-l)}Fe$ (33)			
$T'H_{(4-m)}Fe_2 \rightleftharpoons T''H_{(4-l)}Fe_2$ (34)			
$T'H_{(4-m)}Fe + Fe \rightleftharpoons L + T'H_{(4-l)}Fe_2$ (35)			
$T_CH_3 + Fe^{3+} \rightleftharpoons T_CH_3Fe$ (36)			$\sim 1 \times 10^{-16}$ M

[a] Reactions 26 and 36 are written to introduce equilibrium constants independent of the ligand nature. j is unknown. $l = 2$ or 3 (*15*).

Table 2: Mechanisms of Interaction of Bismuth-Loaded and Iron-Loaded Human Serum Transferrin with Transferrin Receptor 1[a]

reaction	direct rate constant	reverse rate constant	equilibrium constant
$TFR + H^+ \rightleftharpoons TFRH$ (18)			10 nM (*7*)
interaction with TBi_2			
$TFR + TBi_2 \rightleftharpoons TRF{-}TBi_2$ (19)	$(2.2 \pm 1.5) \times 10^8\ M^{-1}\ s^{-1}$	$900 \pm 400\ s^{-1}$	$4 \pm 0.4\ \mu$M
interaction with TFe_2 (*7*)			
$TFR + TFe_2 \rightleftharpoons (TFR{-}TFe_2)'$ (37)	$3.2 \times 10^{10}\ M^{-1}\ s^{-1}$	$1.6 \times 10^4\ s^{-1}$	0.5 μM
$(TFR{-}TFe_2)' \rightleftharpoons TFR{-}TFe_2$ (38)			4.6×10^{-3}
$TFR + TFe_2 \rightleftharpoons TFR{-}TFe_2$ (39)			2.3 nM

[a] Reaction 39 is written to introduce the overall dissociation constant of the holo-ST−TFR adduct.

complexes with nitrogen- and/or oxygen-containing ligands (*18*). The ligands involved in formation of a complex with Fe(III) and transferrins are four oxygen-containing ligands (two phenolates of two tyrosines, the carboxylate of an aspartate, and a carbonate which acts as a synergistic anion) and the nitrogen-containing imidazole of a histidine (*4*, *5*). Bi(III) forms stable complexes with transferrins and has the same protein ligands, including the synergistic carbonate (*10*). Nevertheless, the mechanism of complex formation between ST and Bi(III) differs from that of the same protein with Fe(III). Indeed, upon formation of a complex with Fe(III), transferrin is changed from an iron-free open structure to an iron-loaded closed structure in which iron becomes imprisoned in a cleft where the Fe(III) complex is in a distorted octahedral geometry (*4*, *5*). This geometry cannot be adapted to Bi(III) which has a much larger ionic radius than iron. The transferrin−bismuth complex would, therefore, be expected to be formed by mechanisms different from those reported for iron. The transition from an open to a closed conformation of ST upon iron uptake occurs in ~1 h (*15*). The final process detected during bismuth uptake is finished in ~50 s (Figure 1A). This process cannot, therefore, depict a similar transition from open to closed as for iron. This probably implies, as already suggested in the literature, that the Bi−ST complex has a structure different from that of holotransferrin, with probably the bismuth-loaded protein not achieving the same closed conformation (*10*).

Bismuth is widely used in medicine (*18*). Although transferrins are considered the most probable target of bismuth in the organism (*33*), the means of its incorporation and transport are still unknown. The fact that Bi(III) forms stable complexes with transferrin led to the hypothesis of its possible incorporation by the iron acquisition pathway (*10*−*12*, *33*, *34*). Nevertheless, formation of a complex between a metal cation (e.g., Cu^{2+} and Al^{3+}) and transferrin does not necessarily signify that the metal-loaded protein interacts with TFR. Indeed, copper forms a stable complex with transferrin, and its incorporation does not follow the iron acquisition pathway (*35*). Al(III) also forms a stable complex with ST which does not interact with TFR and probably does not follow the iron acquisition pathway (*9*, *36*).

In Table 2, we summarize the mechanism of interaction of Bi_2ST with TFR and compare it to that of holo-ST. The mechanism of interaction of the Bi-loaded transferrin with TFR is a single step-process (eq 19), whereas that with holo-ST is a two-step process (eqs 37 and 38). Moreover, the thermodynamic stability of the TBi_2−TFR complex (4 μM, eq 19, Table 2) is ~3 orders of magnitude lower than the overall stability of the holo-ST−TFR complex (2.3 nM, eq 39, Table 2). Does this imply that the interaction between the two proteins occurs on sites different from those involved in formation of the TFR−holo-ST adduct? We have shown by temperature-jump experiments performed on mixtures of the TBi_2−TFR complex and TFe_2 or the TFe_2−TFR complex and TBi_2, all in a thermodynamically equilibrated state, that equilibrium is always very rapidly and totally shifted toward the TFe_2−TFR species. This suggests that the interaction

between TBi_2 and TFR occurs at least partly at the same binding sites of TFe_2.

The site of binding of holotransferrin to the soluble ectodomain of TFR is now well delimited (*21*, *37*). However, our results deal with the complete TFR in the presence of CHAPS micelles (*7*). These can play the role of an artificial membrane where the endodmain of the protein is in interaction with the micelle and the ectodomain directed toward the aqueous medium (*7*). We should, therefore, be cautious in transposing our results with those reported for the separate soluble ectodomain of TFR, in which the C-site of holo-ST seems to bind residues in the helical domain (*20*, *38*). These residues are also common with those of the interaction of HFE with TFR (*21*, *39*−*41*). There is, furthermore, a probable interaction of holotransferrin with the protease-like domain (*21*), which, however, does not seem to be involved in the interaction with HFE (*21*). This, in addition to the work of Cheng et al., tends to indicate that there are two binding sites on a receptor subunit, one in the helical domain, common to mainly the C-site of holo-ST and HFE, and the other in the protease-like domain, specific to holo-ST (*20*, *21*, *38*). Only the binding site common to HFE and holo-ST is assumed to interact with the C-site of holotransferrin, whereas the N-site interacts with the protease-like domain (*20*). The binding of holo-ST to TFR occurs in two steps. The first is practically instantaneous (50 μs) and corresponds to a molecular interaction between the two proteins to yield the $(TFR-Fe_2)'$ intermediate product with a dissociation constant of 0.5 μM (eq 37, Table 2). The second is a very slow (8000 s) change in the conformation of the $(TFR-Fe_2)'$ product to yield the final $TFR-Fe_2$ product (eq 38, Table 2). If we transpose the findings of Cheng et al. (*20*) with our mechanism (*7*), the first fast step would be the interaction of the C-site of holo-ST with the helical domain of TFR and the second slow step would involve the change in conformation of holo-ST, the C-site of which is interacting with TFR to allow the N-site to interact with the protease-like domain which stabilizes further the protein−protein adduct (*7*). However, iron acquisition via receptor-mediated endocytosis is completed in a few minutes and occurs immediately after the interaction of TFe_2 with TFR (*1*, *2*, *6*). This implies that most of the iron would be transported into the cytosol before the $TFR-TFe_2$ complex attains its final equilibrated state (eq 38, Table 2). This transport would, therefore, mainly involve the kinetic $(TFR-TFe_2)'$ intermediate (Table 2). Furthermore, the affinity of TFR for TBi_2 is ($K_d^{-1} = 2.2 \times 10^5$ M^{-1}, eq 19, Table 2) only ~1 order of magnitude lower than that reported for the first step of the interaction of TFR with holo-ST at the end of the first instantaneous kinetic step (2×10^6 M^{-1}, eq 37, Table 2). Although 10 times slower than the formation of the holo-ST−TFR intermediate (eq 19, Table 2), the interaction of the bismuth-loaded ST with TFR involves the same loss of a proton from the receptor and seems to occur partly on the same site as the first step of the interaction with TFe_2 (eqs 18, 19, and 37, Table 2). The slow change in conformation (eq 38, Table 2) that follows the interaction of holo-ST with TFR is not detected with TBi_2. This suggests that the bismuth-loaded transferrin may not interact with the protease-like domain of TFR. Nonetheless, the fact that the slow process was not detected by our means of investigation does not necessarily imply its absence.

The competition between holo-ST and Bi_2T toward the interaction with TFR is kinetically and thermodynamically in favor of holo-ST. This is confirmed by the equilibrium and the rate constants for each of the two mechanisms (Table 2). Subsequently, the interaction between TFR and bismuth-loaded transferrin would only occur if the T_2Bi concentration is high as than that of holo-ST. This can be the case during bismuth therapy when large amounts of bismuth salts are administered daily (*42*). Since ST saturation with iron does not exceed 40% in the blood stream (*1*, *2*), uptake of bismuth by transferrin can occur rapidly with apo-ST according to the mechanism in Table 1. Furthermore, the interaction of TBi_2 with TFR would also occur very rapidly by the mechanism in Table 2. However, we should keep in mind that all our results were acquired *in vitro* and cannot, therefore, be directly transposed into a living organism.

CONCLUSION

In this article, we propose, in cell-free assays, a mechanism for exchange of bismuth between the nitrilotriacetate ligand and human serum transferrin, and show that the bismuth-loaded transferrin interacts with the transferrin receptor. Is this sufficient to imply that bismuth incorporation follows the receptor-mediated acquisition pathway? This question cannot be answered at this stage.

REFERENCES

1. Aisen, P., Enns, C., and Wessling-Resnick, M. (2001) Chemistry and biology of eukariotic iron metabolism, *Int. Biochem. Cell Biol. 10*, 940−959.
2. Crichton, R. (2001) *Inorganic Biochemistry of Iron Metabolism*, J. Wiley and Sons, New York.
3. Bruns, C. M., Nowalk, A. J., Arvai, A. S., McTigue, M. A., Vaughan, K. G., Mietzner, T. A., and McRee, D. E. (1997) Structure of *Haemophilus influenzae* Fe^{3+}-binding protein reveals convergent evolution within a superfamily, *Nat. Struct. Biol. 4*, 919−924.
4. Zuccola, H. J. (1992) The crystal structure of monoferric human serum transferrin, Ph.D. Thesis, Georgia Institute of Technology, Atlanta.
5. Moore, S. A., Anderson, B. F., Groom, C. R., Haridas, M., and Baker, E. N. (1997) Three-dimensional structure of diferric bovine lactoferrin at 2.8 Å resolution, *J. Mol. Biol. 274*, 222−236.
6. Dautry-Varsat, A., Ciechanover, A., and Lodish, H. F. (1982) pH and recycling of transferrin during receptor-mediated endocytosis, *Proc. Natl. Acad. Sci. U.S.A. 80*, 2258−2262.
7. Hémadi, M., Kahn, P. H., Miquel, G., and El Hage Chahine, J. M. (2004) Transferrin's mechanism of interaction with receptor 1, *Biochemistry 43*, 1736−1745.
8. Harris, W. R. (1989) Equilibrium constants for the complexation of metal ions by serum transferrin, *Adv. Exp. Med. Biol. 249*, 67−93.
9. Hémadi, M., Kahn, P. H., Miquel, G., and El Hage Chahine, J. M. (2003) Aluminum exchange between citrate and human serum transferrin and interaction with transferrin receptor 1, *Biochemistry 42*, 3120−3130.
10. Li, H., Sadler, P. J., and Sun, H. (1996) Unexpectedly strong binding of a large metal ion (Bi^{3+}) to human serum transferrin, *J. Biol. Chem. 271*, 9483−9489.
11. Zhang, L., Szeto, K. Y., Wong, B. W. B., Loh, T. T., Sadler, P. J., and Sun, H. (2001) Interaction of bismuth with human lactoferrin and recognition of the Bi^{III}-lactoferrin complex by intestinal cells, *Biochemistry 40*, 13281−13287.
12. Sun, H., Li, H., Masson, A. B., Woodworth, R. C., and Sadler, P. J. (1999) N-Lobe versus C-lobe complexation of bismuth by human transferrin, *Biochem. J. 337*, 105−111.
13. Yokel, R. A., Allen, D. D., and Ackley, D. C. (1999) The distribution of aluminum into and out of the brain, *J. Inorg. Biochem. 76*, 127−132.

14. Smith, C. A., Anderson, B. F., Baker, H. M., and Baker, E. N. (1992) Metal substitution in transferrins: the crystal structure of human copper lactoferrin, *Biochemistry 31*, 4527−4533.
15. Pakdaman, R., Bou Abdallah, F., and El Hage Chahine, J. M. (1999) Transferrin: is a mixed chelate-protein ternary complex involved in the mechanism of iron uptake by serum-transferrin in vitro? *J. Mol. Biol. 293*, 1273−1284.
16. Pakdaman, R., Petitjean, M., and El Hage Chahine, J. M. (1998) Transferrins, a mechanism of iron uptake by lactoferrin, *Eur. J. Biochem. 254*, 144−153.
17. Bou Abdallah, F., and El Hage Chahine, J. M. (1998) Transferrins: hen ovo-transferrin, interaction with bicarbonate and iron uptake, *Eur. J. Biochem. 258*, 1022−1031.
18. Sadler, P. J., and Sun, H. (1999) Coordination chemistry of metals in medicine: target sites for bismuth, *Coord. Chem. Rev. 185*−*186*, 689−709.
19. Lawrence, C. M., Ray, S., Babyonyshev, M., Galluster, R., Brhani, B. W., and Harrison, S. C. (1999) Crystal structure of the ectodomain of human transferrin receptor, *Science 286*, 779−782.
20. Cheng, Y., Zak, O., Aisen, P., Harrison, S. C., and Walz, T. (2004) Structure of the human transferrin receptor-transferrin complex, *Cell 116*, 565−576.
21. Giannetti, A. M., Snow, P. M., Zak, O., and Bjorkman, P. J. (2003) Mechanism for multiple ligand recognition by the human transferrin receptor, *PLoS Biol. 1*, 341−350.
22. Eigen, M., and DeMaeyer, L. (1963) Relaxation methods, in *Techniques of Organic Chemistry: Investigation of Rates and Mechanism of Reactions, part II* (Friess, S. L., Lewis, E. S., and Weissberger, A., Eds.) Vol. 8, pp 895−1029, Wiley-Interscience, New York.
23. Bernasconi, C. F. (1976) *Relaxation Kinetics*, Academic Press, New York.
24. El Hage Chahine, J. M., and Fain, D. (1993) The mechanism of iron transferrin interactions: Uptake of the iron nitrilotriacetic acid complex, *J. Chem. Soc., Dalton Trans.*, 3137−3143.
25. Summers, S. P., Abboud, K. H., Farrah, S. R., and Palenik, G. J. (1994) Syntheses and structures of bismuth(III) complexes with nitrilotriacetic acid, ethylenediaminetetraacetic acid, and diethylenetriaminepentaacetic acid, *Inorg. Chem. 33*, 88−92.
26. Asato, E., Kamamuta, K., Imade, R., and Yamasaki, M. (2000) Solution structures and ligand exchange dynamics of bismuth(III) complexes with nitrilotriacetic acid and N-(2-hydroxyethyl)-iminodiacetic acid, in *Inorganic Reaction Mechanisms*, Vol. 2, pp 57−68, Gordon and Breach, Amsterdam.
27. Makey, D. G., and Seal, U. S. (1976) The detection of four molecular forms of human transferrin during the iron binding process, *Biochim. Biophys. Acta 453*, 250−256.
28. Turkewitz, A. P., Amatruda, J. F., Borhani, D., Harrison, S. C., and Schwartz, A. L. (1988) High yield purification of the human transferrin receptor and properties of its major extracellular fragment, *J. Biol. Chem. 263*, 8318−8325.
29. Bali, P. K., Zak, O., and Aisen, P. (1991) A new role for the transferrin receptor in the release of iron from transferrin, *Biochemistry 30*, 324−328.
30. Bellounis, L., Pakdaman, R., and El Hage Chahine, J. M. (1996) Apotransferrin proton dissociation and interactions with bicarbonate in neutral media, *J. Phys. Org. Chem. 9*, 111−118.
31. Martell, A. E., and Smith, R. M. S. (1982) *Critical Stability Constants*, Vol. 5, Plenum Press, New York.
32. Pearson, R. G. (1963) Hard and soft acids and bases, *J. Am. Chem. Soc. 85*, 3533−3539.
33. Sun, H., and Szeto, K. Y. (2003) Binding of bismuth to serum proteins: implication for targets of Bi(III) in blood plasma, *J. Inorg. Biochem. 94*, 114−120.
34. Sun, H., Li, H., Mason, A. B., Woodworth, R. C., and Sadler, P. J. (2001) Competitive binding of bismuth to transferrin and albumin in aqueous solution and blood plasma, *J. Biol. Chem. 276*, 8829−8835.
35. Lee, J., Pena, M. M., Nose, Y., and Thiele, D. J. (2002) Biochemical characterization of the human copper transporter Ctrl1, *J. Biol. Chem. 277*, 4380−4387.
36. Harris, W. R., Wang, Z., and Hamada, Y. Z. (2003) Competition between transferrin and serum ligands citrate and phosphate for the binding of aluminum, *Inorg. Chem. 42*, 3262−3273.
37. Dubljevic, V., Sali, A., and Goding, J. W. (1999) A conserved RGD (Arg-Gly-Asp) motif in the transferrin receptor is required for binding to transferrin, *Biochem. J. 341*, 11−14.
38. Liu, R., Quan, J.-Q., Zak, O., Aisen, P., and Chance, M. R. (2003) Structural reorganization of the transferrin-C lobe and transferrin receptor upon complex formation: The C-lobe binds to the receptor helical domain, *Biochemistry 42*, 12447−12454.
39. Lebron, J. A., West, A. P., and Bjorkman, P. J. (1999) The hemochromatosis protein HFE competes with transferrin for binding to the transferrin receptor, *J. Mol. Biol. 294*, 239−245.
40. Bennet, M. J., Lebron, J. A., and Bjorkman, P. J. (2000) Crystal structure of the hereditary haemochromatosis protein HFE complexed with the transferrin receptor, *Nature 403*, 46−53.
41. Gianneti, A. M., and Bjorkman, P. J. (2004) HFE and transferrin directly compete for transferrin receptor in solution and at the cell surface, *J. Biol. Chem. 279*, 25866−25875.
42. Spenard, J., Aumais, C., Massicotte, J., Tremblay, C., and Lefebvre, M. (2004) Influence of omeprazole on bioavailability of bismuth following administration of a triple capsule of bismuth biskalcitrate, metronidazole, and tetracycline, *J. Clin. Pharmacol. 44*, 640−645.

BI048484P